Supporting Information:

Structural Determination of a Metastable Ag_{27} Nanocluster and Its Transformation into Ag_8 and Ag_{29} Nanoclusters

Chen Zhu,[1,2,#] Tengfei Duan,[3,#] Xiao Wei,[1,2] Hao Li,[1,2] Xi Kang,[1,2,*] Yong Pei,[3,*] Manzhou Zhu[1,2,*]

[1]Department of Chemistry and Centre for Atomic Engineering of Advanced Materials, Anhui Province Key Laboratory of Chemistry for Inorganic/Organic Hybrid Functionalized Materials, Anhui University, Hefei 230601, P. R. China.

[2]Key Laboratory of Structure and Functional Regulation of Hybrid Materials, Anhui University, Ministry of Education, Hefei 230601, P. R. China.

[3]Department of Chemistry, Key Laboratory of Environmentally Friendly Chemistry and Applications of Ministry of Education, Xiangtan University, Hunan Province, China, P. R. China.

[#]C.Z. and T.D. contributed equally.

*E-mails of corresponding authors: kangxi_chem@ahu.edu.cn (X.K.); ypei2@xtu.edu.cn (Y.P.); zmz@ahu.edu.cn (M.Z.)

Notes: The authors declare no competing financial interest.

This Supporting Information includes:

Figures S1-S12

Tables S1-S3

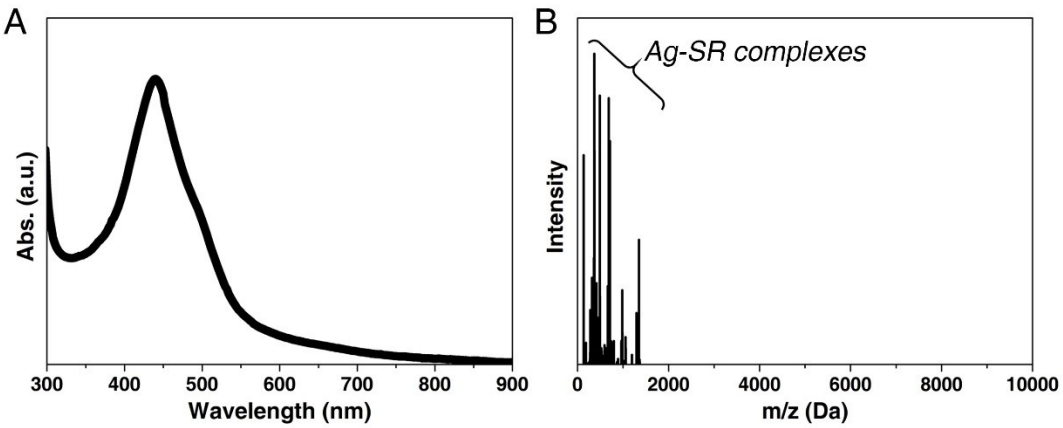

Fig. S1 (A) UV-vis spectrum and (B) ESI-MS result of the prepared products for the synthesis of Ag_{27} in the absence of DPPM. No optical absorption and mass signal of the Ag_{27} nanocluster was observed, while several mass peaks of Ag-SR complexes were detected.

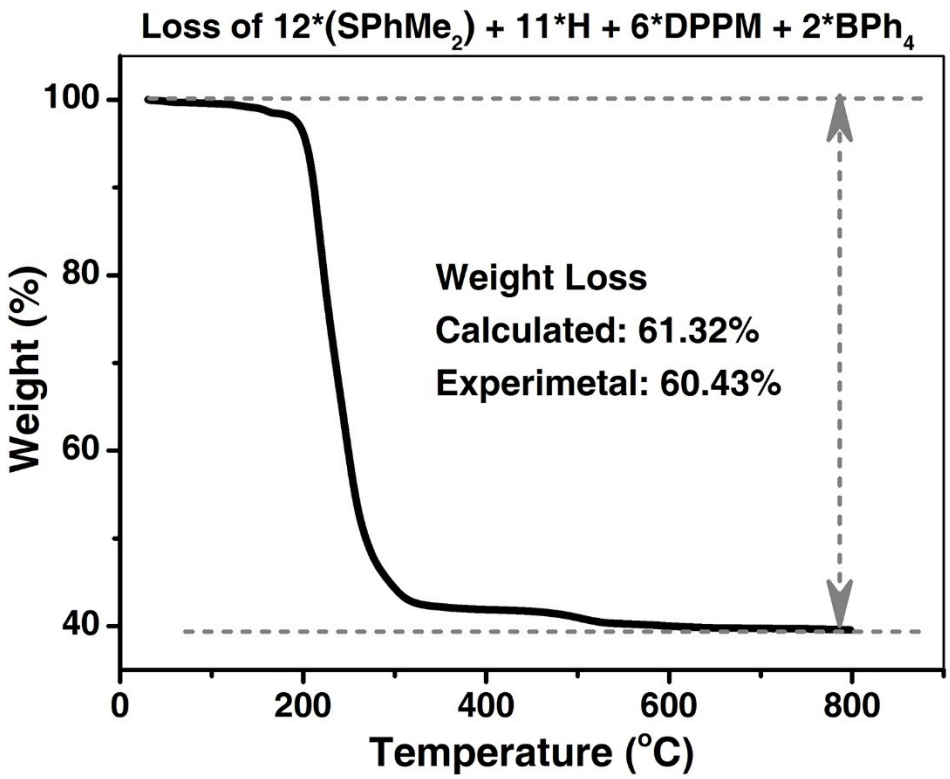

Fig. S2 TGA result of $[Ag_{27}H_{11}(SPhMe_2)_{12}(DPPM)_6](BPh_4)_2$.

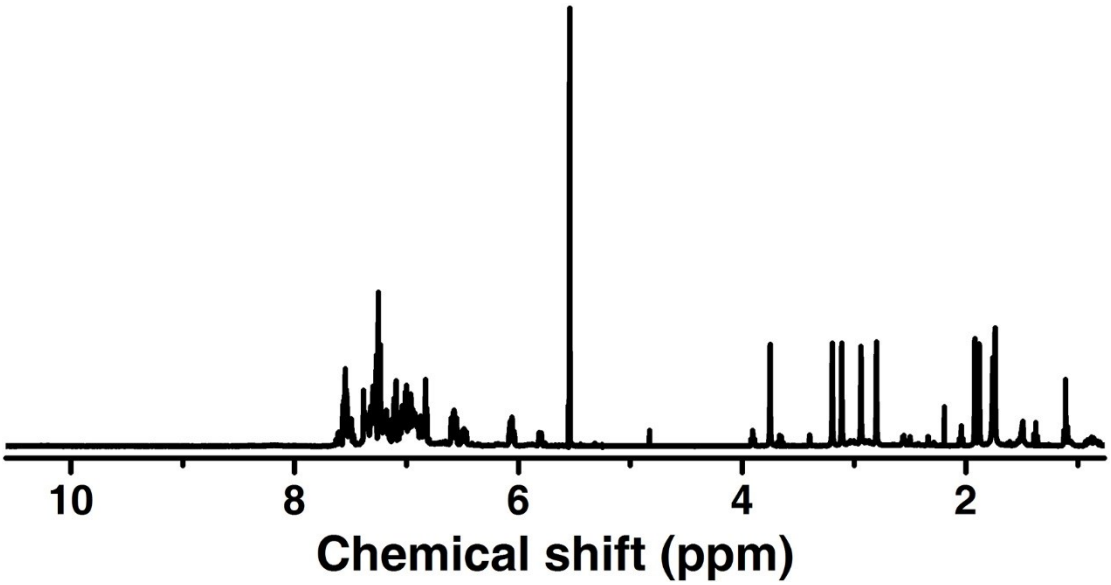

Fig. S3 ^{1}H NMR spectrum of the $[Ag_{27}H_{11}(SPhMe_2)_{12}(DPPM)_6]^{2+}$ nanocluster dissolved in CD_2Cl_2. The signal of CH_2Cl_2 locates at 5.7 ppm.

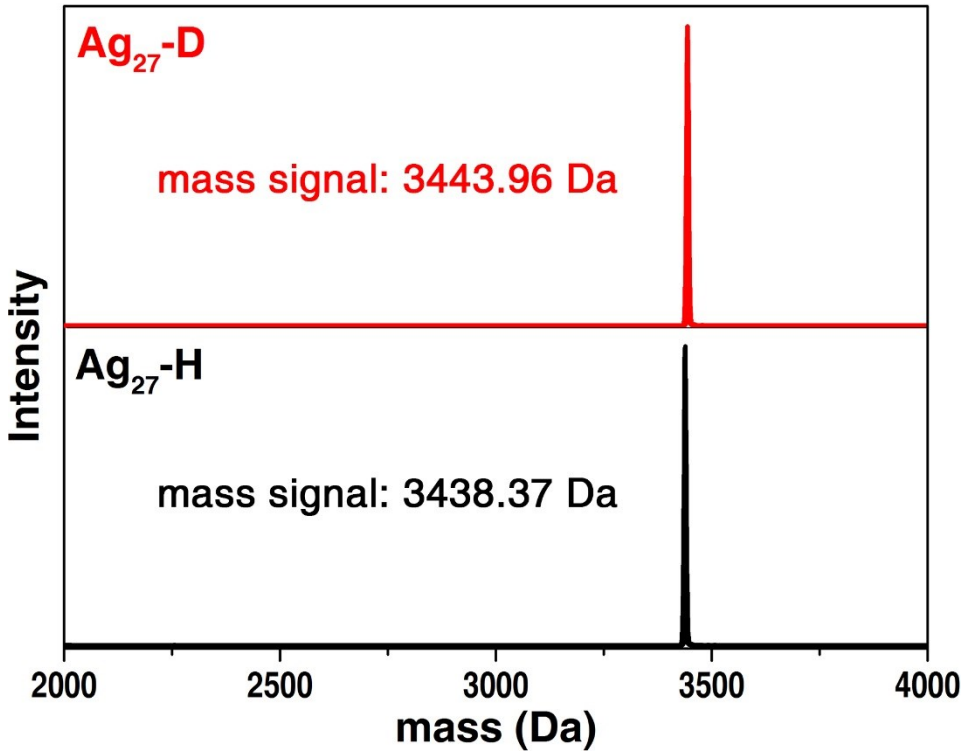

Fig. S4 ESI-MS results of $[Ag_{27}H_{11}(SPhMe_2)_{12}(DPPM)_6]^{2+}$ (black line) and $[Ag_{27}D_{11}(SPhMe_2)_{12}(DPPM)_6]^{2+}$ (red line) in a mass range between 2000 to 4000 Da.

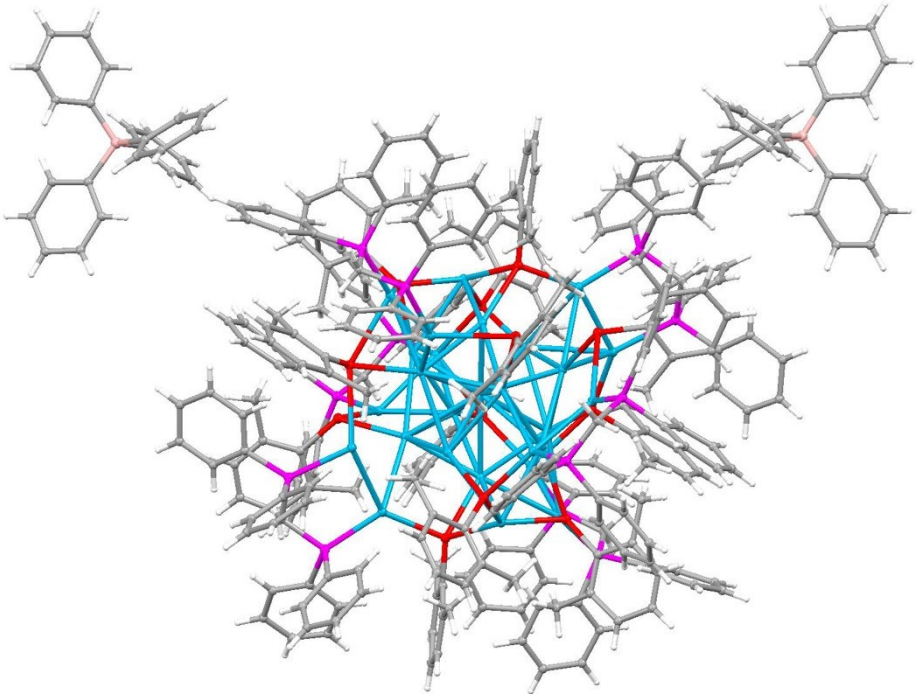

Fig. S5 The total structure of $[Ag_{27}H_{11}(SPhMe_2)_{12}(DPPM)_6](BPh_4)_2$ with no hydride ligands. Color legends: light blue sphere, Ag; red sphere, S; magenta sphere, P; pink sphere, B; grey sphere, C; white sphere, H.

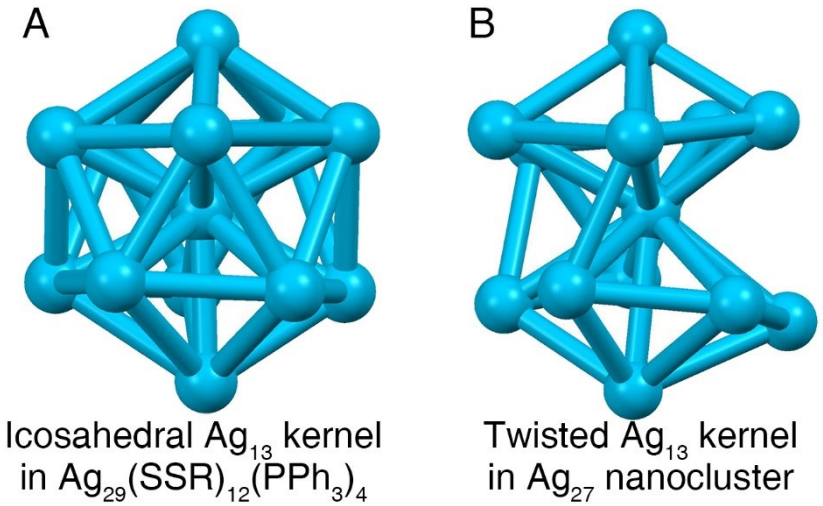

Fig. S6 Structure comparison between (A) the icosahedral Ag_{13} kernel of the $Ag_{29}(SSR)_{12}(PPh_3)_4$ nanocluster and (B) the twisted Ag_{13} kernel of the $Ag_{27}H_{11}(SPhMe_2)_{12}(DPPM)_6$ nanocluster. The detailed comparison is shown in Table S1.

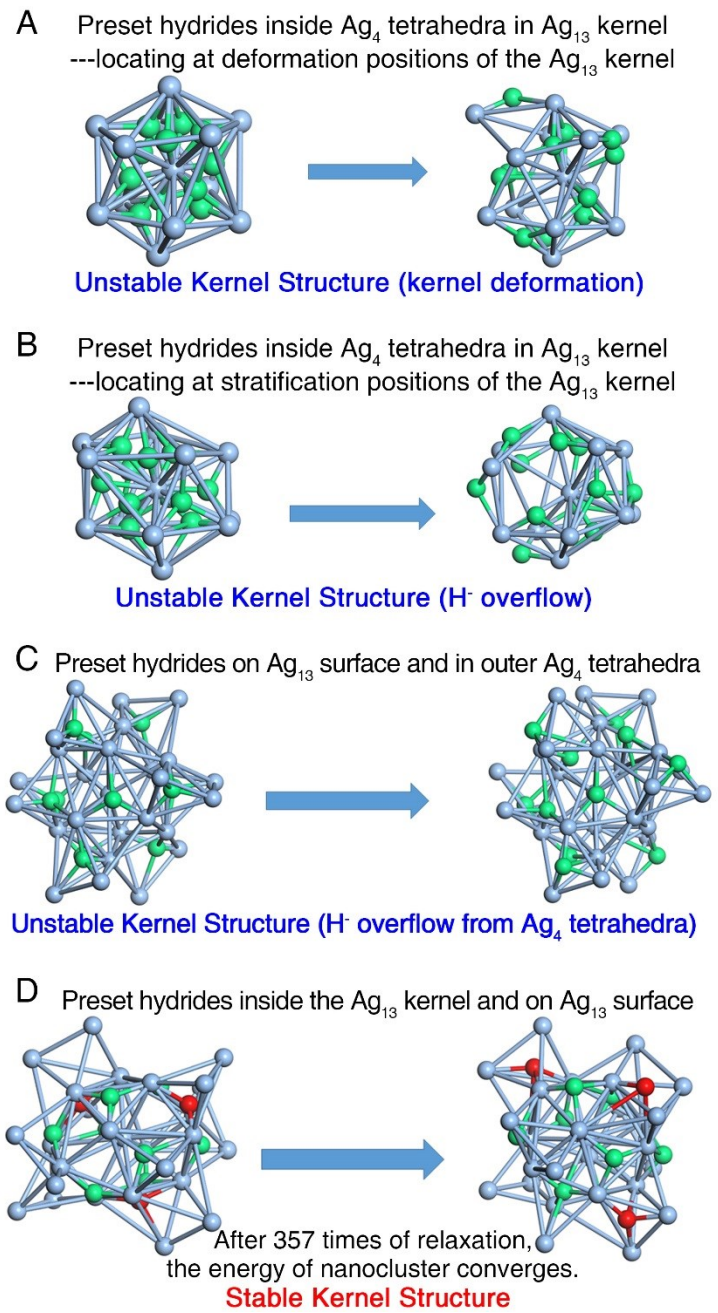

Fig. S7 Theoretical results of the locations of hydrides in $Ag_{27}H_{11}(SPhMe_2)_{12}(DPPM)_6$. (A) The hydrides are preset inside Ag_4 tetrahedra in the Ag_{13} kernel (mainly locating the stratification positions), while the kernel structure is unstable and would deform after relaxation. (B) The hydrides are preset inside Ag_4 tetrahedra in the Ag_{13} kernel (mainly locating the deformation positions), while the kernel structure is unstable the hydrides would overflow from the kernel after relaxation. (C) The hydrides are preset on the Ag_{13} kernel surface and inside the outer Ag_4 tetrahedra, while the kernel structure is unstable the hydrides would overflow from the outer Ag_4 tetrahedra after relaxation. (D) The hydrides are preset inside the Ag_{13} kernel and in the Ag_{13} kernel surface. After 356 times of relaxation, the energy of the final structure converges, demonstrating the stability of the structure.

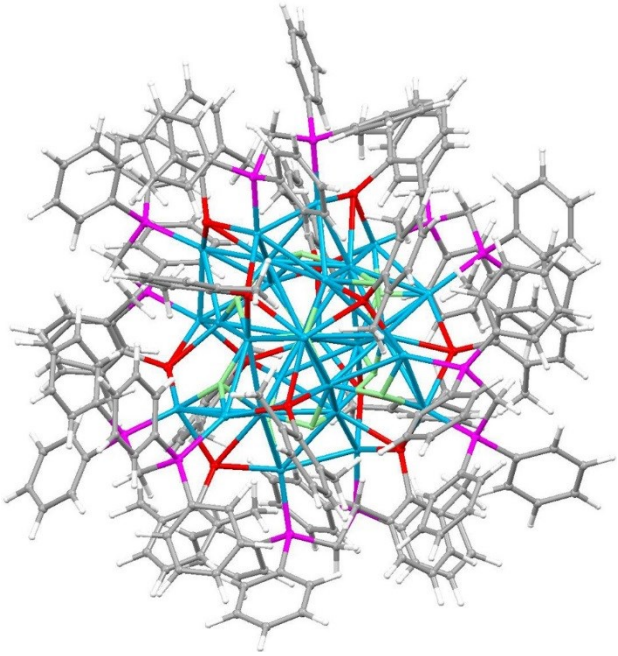

Fig. S8 The total structure of $[Ag_{27}H_{11}(SPhMe_2)_{12}(DPPM)_6]^{2+}$. Color legends: light blue sphere, Ag; red sphere, S; magenta sphere, P; light green sphere, hydride; grey sphere, C; white sphere, H.

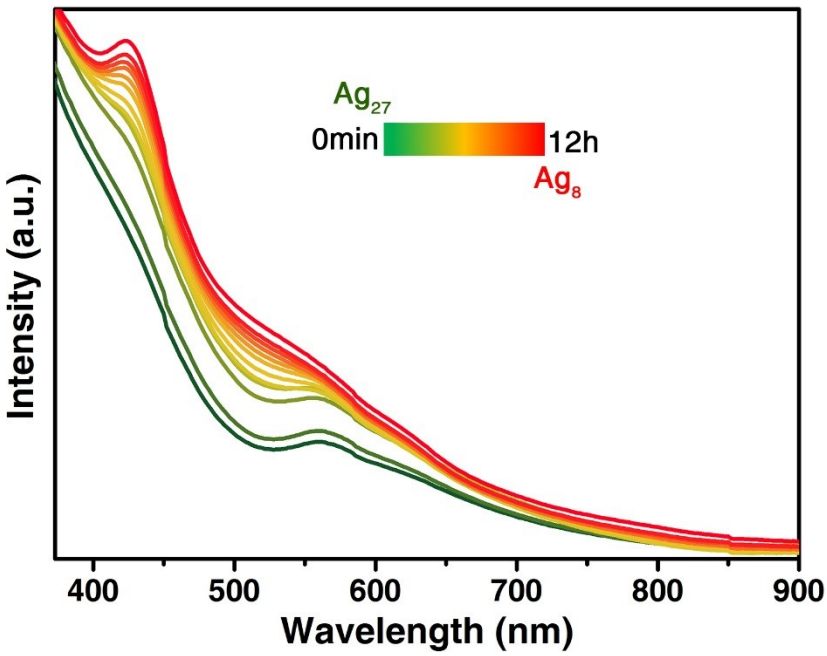

Fig. S9 Time-dependent UV-vis of the Ag_{27} nanocluster in the presence of H^- (by adding the 3mL of CH_3CH_2OH solution of 3mg of $NaBH_4$ into 20mL of CH_2Cl_2 solution of 20mg of Ag_{27}-H). The final optical absorption demonstrated the generation of the Ag_8 nanocluster.

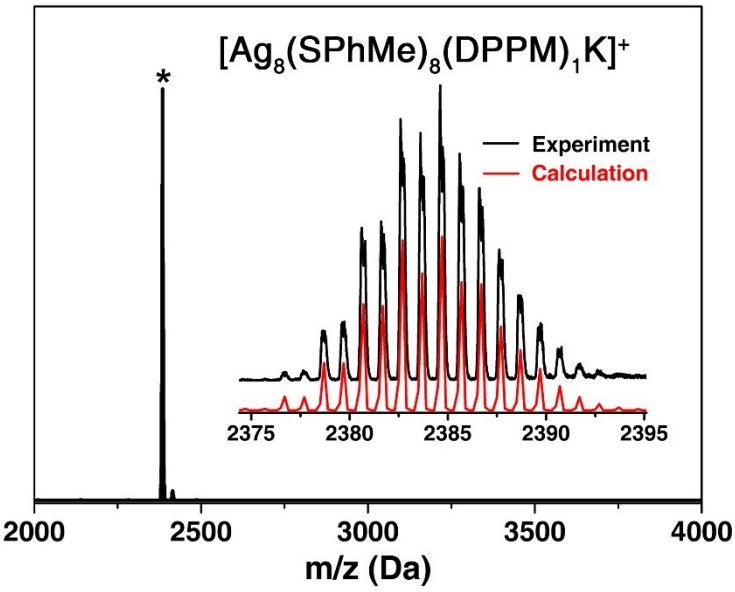

Fig. S10 ESI-MS spectrum in 2000-4000 Da mass range of the $Ag_8(SPhMe_2)_8(DPPM)_1$ nanocluster. Insets: the experimental (black) and calculated (red) isotope patterns of the $[Ag_8(SPhMe_2)_8(DPPM)_1K]^+$.

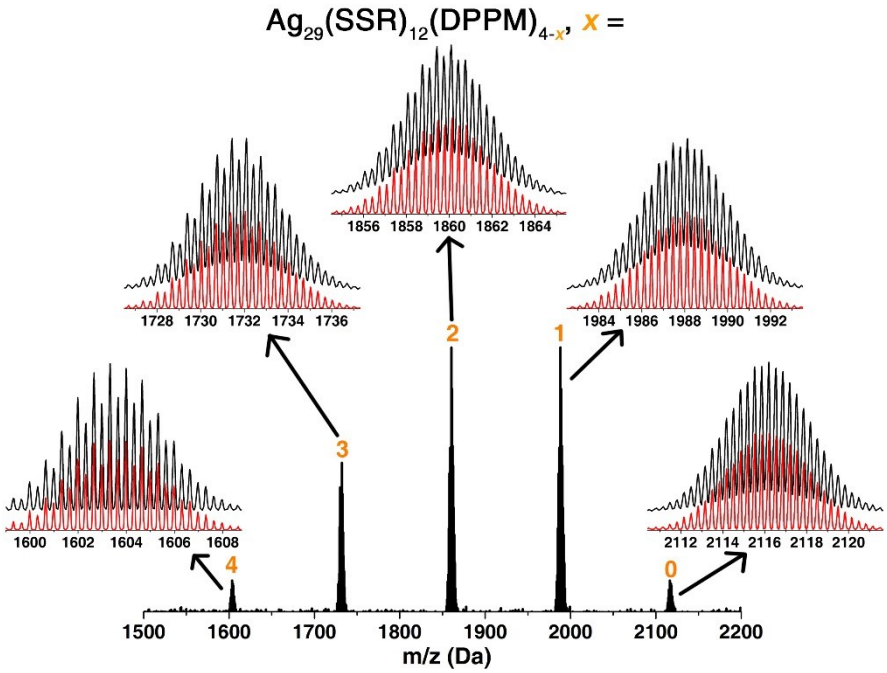

Fig. S11 ESI-MS spectrum in 1500-2200 Da mass range of the $Ag_{29}(SSR)_{12}(DPPM)_4$ nanocluster. Insets: the experimental (black) and calculated (red) isotope patterns of $Ag_{29}(SSR)_{12}(DPPM)_4$ nanocluster and its dissociated products.

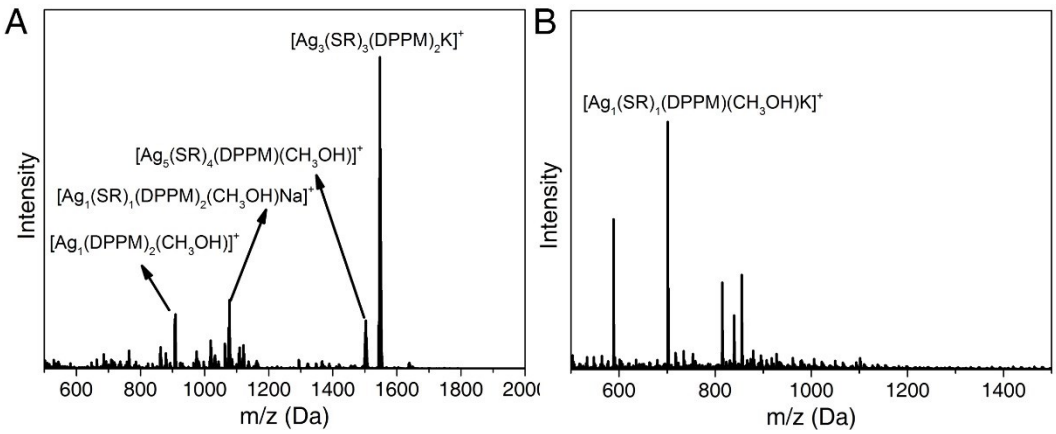

Fig. S12 (A) ESI-MS results (at a low mass range, in a positive mode) of the transformation from Ag_{27} to Ag_8 to detect the by-products. Several mass signals of by-products were observed, including $[Ag_1(DPPM)_2(CH_3OH)_1]^+$, $[Ag_1(SR)_1(DPPM)_2(CH_3OH)_1Na_1]^+$, $[Ag_5(SR)_4(DPPM)_1(CH_3OH)]^+$, and $[Ag_3(SR)_3(DPPM)_2K_1]^+$. SR = $SPhMe_2$. No mass peak was detected in the negative mode at a range from 500-1500 Da. (B) ESI-MS results (at a low mass range, in a positive mode) of the transformation from Ag_{27} to Ag_{29} to detect the by-products. A mass signal of by-product was observed, i.e., $[Ag_1(SR)_1(DPPM)_1(CH_3OH)_1K_1]^+$. SR = $SPhMe_2$. The other peaks were not assigned. No mass peak was detected in the negative mode at a range from 500-1500 Da.

Table S1. Comparison of Ag---Ag bond lengths between the icosahedral Ag_{13} kernel of the $Ag_{29}(SSR)_{12}(PPh_3)_4$ nanocluster and the twisted Ag_{13} kernel of the $Ag_{27}H_{11}(SPhMe_2)_{12}(DPPM)_6$ nanocluster. The comparison corresponds to Figure S5.

Kernel	Icosahedral Ag_{13} kernel (Ag_{29} nanocluster)	Twisted Ag_{13} kernel (Ag_{27} nanocluster)
Bond lengths	2.761-2.975 Å	2.835-3.206 Å
Avg.	2.868 Å	2.993 Å

Table S2. Comparison of the bond lengths between different Ag---H in $Ag_{27}H_{11}(SPhMe_2)_{12}(DPPM)_6$.

Coordination modes	μ_2-H---Ag	μ_3-H---Ag	μ_4-H---Ag
Bond lengths	1.754-1.840 Å	1.837-2.128 Å	1.909-2.098 Å
Avg.	1.822 Å	1.940 Å	2.029 Å

Table S3. Crystal data and structure refinement for the $[Ag_{27}H_{11}(SPhMe_2)_{12}(DPPM)_6](BPh_4)_2$ nanocluster.

Crystal system	triclinic
Space group	P -1
a/Å	18.5850(4)
b/Å	20.8944(4)
c/Å	42.1406(7)
α/°	98.8620(10)
β/°	95.6380(10)
γ/°	91.5050(10)
Volume/Å^3	16076.3(5)
Z	2
ρcalcg/cm^3	1.550
μ/mm^{-1}	14.485
F(000)	7390
Radiation	CuKα (λ = 1.54186)
Index ranges	$-21 \le h \le 17$, $-24 \le k \le 18$, $-48 \le l \le 48$
Final R indexes [I>=2σ (I)]	R1 = 0.0983, wR2 = 0.2733
Final R indexes [all data]	R1 = 0.1237, wR2 = 0.3127